PHYSICAL REVIEW B **86**, 121403(R) (2012)

Spin-polarized edge modes and snake states in HgTe/CdTe quantum wells under an antisymmetric magnetic field

Ying-Tao Zhang,[1] Feng Zhai,[2] Zhenhua Qiao,[3] and Qing-Feng Sun[4]
[1]*College of Physics, Hebei Normal University, Shijiazhuang 050016, China*
[2]*Department of Physics, Zhejiang Normal University, Jinhua 321004, China*
[3]*Department of Physics, The University of Texas at Austin, Austin, Texas 78712, USA*
[4]*Institute of Physics, Chinese Academy of Sciences, Beijing 100190, China*
(Received 15 July 2012; published 17 September 2012)

We demonstrate the effect of an antisymmetric magnetic field on the edge states in inverted HgTe quantum wells using the Landauer-Büttiker formula coupled with the Green's function technique. At any width of the zero-field region, gapless edge modes appear inside the bulk band gap. By calculating the wave function distribution, we find that (i) for Fermi energies inside the bulk gap, the edge states propagate helically along the sample boundaries as a quantum spin-Hall insulator; and (ii) for Fermi energies outside the bulk gap, a pair of states propagate along the boundaries, while the other pair of "snake states" appear and counterpropagate along the central zero-field region. We show numerically that the edge modes in the latter case are robust against the short-range Anderson disorder.

DOI: 10.1103/PhysRevB.86.121403 PACS number(s): 71.20.−b, 72.25.−b, 73.21.Fg, 73.43.Cd

The quantum spin-Hall (QSH) state is a gapless helical edge state that lies inside a bulk insulating gap and is topologically protected.[1–3] Since the proposal of the QSH effect or Z_2 topological insulator in graphene by Kane and Mele,[1,4] its peculiar topological properties have attracted intense interest from both theoretical and experimental communities.[5–7] Due to weak intrinsic spin-orbit coupling,[8] it is difficult to observe the QSH effect in graphene. Fortunately, the QSH state was soon realized in two-dimensional (2D) HgTe/CdTe quantum wells with an inverted electronic structure.[9,10] So far, there has been much progress in searching for 2D topological insulator systems,[11–13] and some of them (e.g., the inverted InAs/GaSb quantum wells[14]) have been confirmed experimentally. Because of their experimental relevance, the helical edge modes and corresponding transport properties of 2D QSH systems have been used to design devices.[15–24] Recently, electron transport properties in HgTe QSH systems under a uniform magnetic field have been broadly investigated.[25–27] However, very little has been done to study the influence of nonuniform magnetic fields on the transport properties of QSH systems.

In this Rapid Communication, we investigate the effect of an antisymmetric perpendicular magnetic field (shown in Fig. 1) on the QSH effect in an inverted HgTe/CdTe quantum well. The magnetic field varies only along the transverse direction (the y axis) of the HgTe waveguide. For simplicity, it is assumed to vanish in a strip of the HgTe waveguide and have the same strength but opposite directions in the upper and lower part of this strip. It is shown that under this kind of magnetic field the helical edge mode still holds inside the bulk band gap. However, when the Fermi energy is located outside the bulk gap, we find that a pair of spin-polarized edge modes are located at sample boundaries propagating from left to right, while the other pair of "snake states" are induced to be localized near the zero-field regime and counterpropagate from right to left. We show numerically that these spin-polarized edge states and snake states are robust against the short-range Anderson disorder.

In the tight-binding representation, the effective four-band Hamiltonian of the HgTe/CdTe quantum well can be written as[9,10,19,28,29]

$$
\begin{aligned}
H = & \sum_{\mathbf{i}} \psi_{\mathbf{i}}^{\dagger} \begin{pmatrix} \epsilon_{\mathbf{i}s} & 0 & 0 & 0 \\ 0 & \epsilon_{\mathbf{i}p} & 0 & 0 \\ 0 & 0 & \epsilon_{\mathbf{i}s} & 0 \\ 0 & 0 & 0 & \epsilon_{\mathbf{i}p} \end{pmatrix} \psi_{\mathbf{i}} \\
& + \left\{ \sum_{\mathbf{i}} \psi_{\mathbf{i}}^{\dagger} \begin{pmatrix} v_{ss} & v_{sp} & 0 & 0 \\ -v_{sp}^{*} & v_{pp} & 0 & 0 \\ 0 & 0 & v_{ss} & v_{sp}^{*} \\ 0 & 0 & -v_{sp} & v_{pp} \end{pmatrix} e^{i\phi_{\mathbf{i},\mathbf{i}+\hat{\mathbf{x}}}} \psi_{\mathbf{i}+\hat{\mathbf{x}}} \right. \\
& + \sum_{\mathbf{i}} \psi_{\mathbf{i}}^{\dagger} \begin{pmatrix} v_{ss} & i v_{sp} & 0 & 0 \\ i v_{sp}^{*} & v_{pp} & 0 & 0 \\ 0 & 0 & v_{ss} & -i v_{sp}^{*} \\ 0 & 0 & -i v_{sp} & v_{pp} \end{pmatrix} e^{i\phi_{\mathbf{i},\mathbf{i}+\hat{\mathbf{y}}}} \psi_{\mathbf{i}+\hat{\mathbf{y}}} \\
& \left. + \text{H.c.} \right\}, \qquad (1)
\end{aligned}
$$

where $\mathbf{i} = (i_x, i_y)$ is the site index, $\psi_{\mathbf{i}} = [a_{\mathbf{i}}, b_{\mathbf{i}}, c_{\mathbf{i}}, d_{\mathbf{i}}]^T$ represents the four annihilation operators of electron on the site $\mathbf{i}$ at the special states $|s, \uparrow\rangle$, $|p_x + ip_y, \uparrow\rangle$, $|s, \downarrow\rangle$, $|-(p_x - ip_y), \downarrow\rangle$, respectively, and $\hat{\mathbf{x}}$, $\hat{\mathbf{y}}$, and $\hat{\mathbf{z}}$ are three unit vectors. In terms of five material-dependent parameters A, B, C, D, and M, the on-site energies ϵ_s and ϵ_p, together with the hopping energies v_{ss}, v_{pp}, and v_{sp}, are expressed as $\epsilon_s = C + M - 4(B + D)/a^2$, $\epsilon_p = C - M - 4(B - D)/a^2$, $v_{ss} = (D + B)/a^2$, $v_{pp} = (D - B)/a^2$, and $v_{sp} = -iA/2a$. The lattice constant of our tight-binding model is taken as $a = 5$ nm. Under the magnetic field $\mathbf{B} = B_z(y)\hat{\mathbf{z}}$, the nearest-neighbor hopping terms acquire a Peierls phase $\phi_{\mathbf{ij}} = \int_{\mathbf{i}}^{\mathbf{j}} \mathbf{A} \cdot d\mathbf{l}/\phi_0$. Here $\mathbf{A} = -\int_{L/2}^{y} B_z(y')dy'\hat{\mathbf{x}}$ is the vector potential and $\phi_0 = \hbar/e$.

 ©2012 American Physical Society

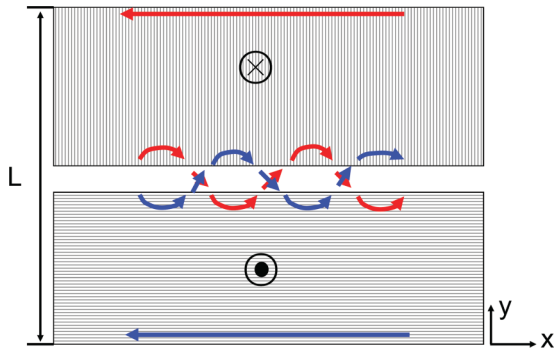

FIG. 1. (Color online) Schematic plot of a HgTe waveguide in the presence of a perpendicular nonuniform magnetic field. The magnetic field vanishes in a strip and has the same strength but opposite directions in the upper and lower part of the strip. The arrows illustrate how the edge modes and snake states propagate in the classical picture.

In the following numerical calculations, the five material parameters for a realistic HgTe/CdTe quantum well are set to be $A = 3.645$ eV Å, $B = -68.6$ eV Å^2, $C = 0$, $D = -51.2$ eV Å^2, and $M = -10$ meV. The waveguide spans the region $0 < y < L$ with $L = 80a$. The strength of the nonuniform magnetic field in the upper region is fixed at $B_u = 0.03\phi_0/a^2$ (=0.79 T). In Fig. 2, we plot the band structures of the system with different widths of the zero-field region [$0a$ in Fig. 2(a) and $20a$ in Fig. 2(b)]. Under a uniform magnetic field, the energy bands of the HgTe waveguide are spin split and the edge states may be gapped.[27] However, the energy spectrum in Fig. 2 is doubly degenerate, and gapless edge modes arise inside the bulk gap. The reason is that the considered system is invariant under the rotation operation

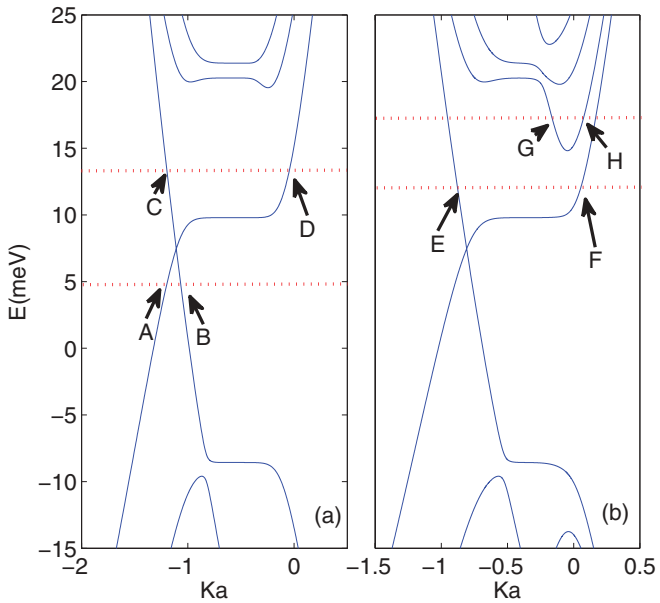

FIG. 2. (Color online) Band energy E vs longitudinal wave vector K for the considered HgTe waveguide with width $L = 80a$. The strength of the nonuniform magnetic field in the upper region is fixed at $B_u = 0.03\phi_0/a^2$. The widths of the zero-field region are $0a$ in (a) and $20a$ in (b), respectively.

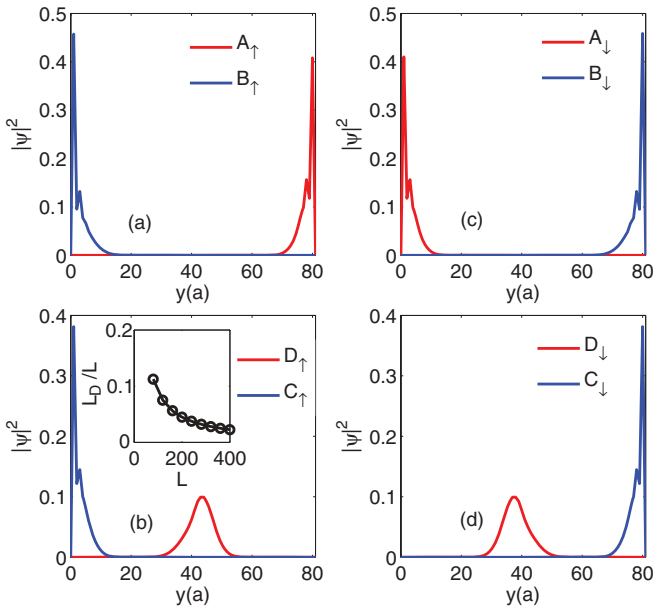

FIG. 3. (Color online) Wave function distribution of states A, B, C, and D labeled in Fig. 2(a). States A, B, and C are localized at the boundary, while state D is localized at the central zero-field regime. The inset in (b) shows the the variation of L_D/L with the waveguide width L, where L_D is the full width at half maximum for the wave function distribution of the spin-up state D.

C_{2x} around the center of the zero-field region. The presence of magnetic fields leads to a series of Landau levels, as shown in Fig. 2(a). When the zero-field region is broadened, the second Landau level is no longer flat and becomes parabolic [see the band labeled with G and H in Fig. 2(b)]. This is distinct from the flat Landau levels under uniform magnetic fields.[27]

For the typical states (A–H) labeled in Fig. 2, the corresponding wave function distributions across the y direction are plotted in Figs. 3 and 4. States A and B lie inside the bulk band gap (in the interval between the first Landau levels of the conduction and valence bands), while states C–H are situated between the first and the second Landau levels of the conduction band. It is seen from Figs. 3(a) and 3(c) that the spin-up and spin-down states of A or B are localized at opposite boundaries, and the opposite spin components of A and B are located at the same boundary. From both the energy dispersion and the edge-state localization, one can conclude that for Fermi energies inside the bulk band gap the helical edge-state propagation resembles that of the QSH effect. Since states B and C belong to the same linear energy spectrum, their wave functions share the similar spin-polarized edge-state propagation. The spin polarization of the helical edge states can be detected as in Ref. 30 via the inverse spin-Hall effect.

In two-dimensional electron gas (2DEG) or graphene systems modulated by an antisymmetric magnetic field, "snake" states can be formed at the interfacial zero-field region.[31–35] Recent resistance measurements on locally gated graphene devices[36] have provided an experimental signature of snake states along a graphene p-n junction. In the considered system there also exist snake states such as D and F–H. The wave function distributions of these states [see Figs. 3(b), 3(d), and 4] are concentrated around the interfacial zero-field region.

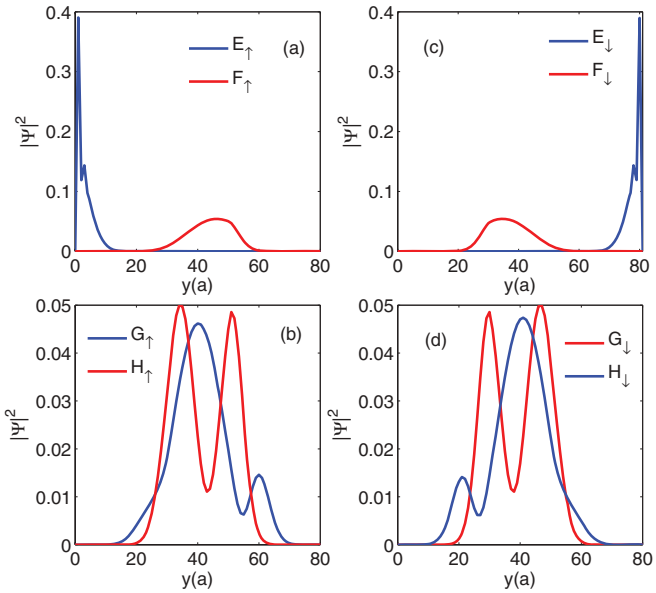

FIG. 4. (Color online) Wave function distribution of states E, F, G, and H labeled in Fig. 2(b). State E is localized at the boundary, while states F, G, and H are localized at the central zero-field regime.

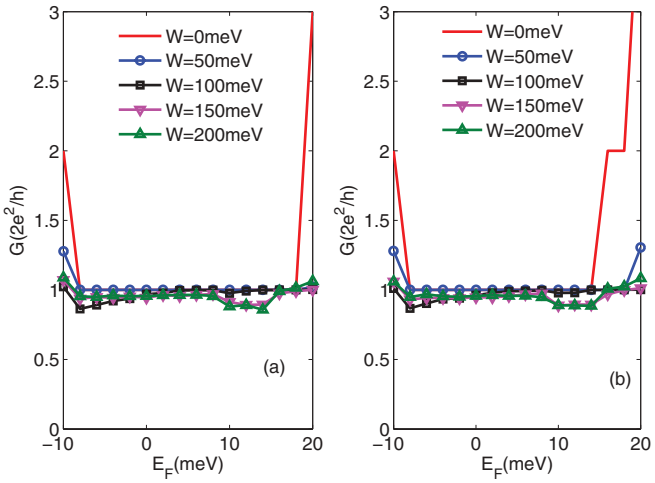

FIG. 5. (Color online) Conductance spectrum under different disorder strengths W. The central scattering region has a length $50a$. Other parameters are the same as Fig. 2.

For the wave function distribution of the snake state such as D [Fig. 3(b)], its full width at half maximum L_D seems to be comparable with the waveguide width L. A finite size scaling shown in the inset of Fig. 3(b) indicates that this state is really localized along the transverse direction of the waveguide. Further, for the states connected with the first (second) Landau level the profile of the wave function has one peak (two peaks). Because the spin-polarized edge states always propagate along the same direction, these snake states are spin dependent in our system, which are distinct from those in 2DEG or graphene. One can see that the spin-up or spin-down snake state keeps spatially mirror symmetric around the central line $y = L/2$ of the sample.

Based on the energy dispersion and the wave function distribution, we can reach a clear picture of the edge modes in the considered system. When the Fermi energy is outside the bulk band gap, one pair of opposite-spin edge states transverse from right to left, while another pair of spin-resolved snake states counterpropagate along the central zero-field region from left to right. This is intuitively illustrated in Fig. 1. For Fermi energy inside the interval between the first Landau levels of the conduction and valence bands, only a helical edge mode exists. The spin-polarized edge modes can be utilized to produce a stable spin bias and spin current.

One may wonder whether the spin-polarized edge states and snake states discussed above are robust against disorders. To this end, in Fig. 5 we explore the disorder effect on the transport properties of the HgTe waveguide under the considered nonuniform magnetic field. To avoid redundant scattering from mismatched interfaces between the semi-infinite leads and the central scattering region, we assume that the total system is described by Eq. (1) with a position-dependent parameter C. In the leads, $C \equiv 0$. In the central region (with size $80a \times 50a$) C is uniformly distributed in the range of $[-W/2, W/2]$, where W measures the disorder strength. The conductance G is obtained from the Landauer-Büttiker formula[37]

$$G = \frac{2e^2}{h}\mathrm{Tr}[\Gamma_R G^r \Gamma_L G^a], \tag{2}$$

where $\Gamma_{R/L} = i(\Sigma^r_{R/L} - \Sigma^a_{R/L})$, $\Sigma^r_{R/L}$ is the self-energy describing the coupling between the right/left semi-infinite lead and the central region,[38] $G^r = (E_F - H_C - \Sigma^r_L - \Sigma^r_R)^{-1}$ is the retarded Green's function, and H_C is the Hamiltonian for the central scattering region.

In the numerical simulation, the conductance G is averaged over up to 500 ensembles. In the absence of disorder ($W = 0$) the conductance shows quantum conductance plateaus in units of $2e^2/h$ [see Fig. 5(a)]. These quantum conductance plateaus are contributed by the spin-polarized edge states and snake states. When the disorder is present, only small fluctuations are imposed on the first conductance plateau $2e^2/h$. Such observations demonstrate that the spin-polarized edge states and snake states are robust against disorder, which is due to their spatial separation. Further, one can see that the strong disorder first destroys the part of the quantum conductance plateau including the contribution of the snake states, then destroys the part of the quantum conductance plateau originated only from the spin-polarized edge states. The reason is that the snake states are distributed in the central region of the sample. The second quantum conductance plateau $4e^2/h$ can be seen in Fig. 5(b), which is contributed partly by states G and H in Fig. 2. From Fig. 4 we know that states G and H are easily destroyed by disorder. Thus the second quantum conductance plateau is destroyed even at a weak disorder $W = 50$ meV.

Finally, we give some remarks. In our setup we take sharp edges for the magnetic fields at the upper and lower parts of the strip. In reality, at both edges the magnetic fields are smooth and even have in-plane components B_{in}. The inclusion of B_{in} introduces only a Zeeman term in Eq. (1). Experimentally, in HgTe/CdTe quantum wells the Zeeman splitting is very small for a magnetic field smaller than 10 T.[39] For the considered magnetic field on the scale $B_u \sim 1$ T, the Zeeman term can be safely omitted. Our antisymmetric magnetic field can be

generated by depositing two parallel ferromagnetic films (with magnetization $\pm M\hat{\mathbf{z}}$) on top of the quantum well. Within the waveguide ($0 < y < L$) the corresponding vector potential can be approximated by $A_x(y) = A_m[1 - \sin(\pi y/L)]$. For this smooth A_x profile with $A_m = B_u a$ our calculations also give snake states and spin-polarized edge states which are similar as those in Figs. 2–4.

In summary, we have investigated the dynamics of electrons in a HgTe/CdTe quantum well in an antisymmetric magnetic field. The energy bands and wave function distribution are calculated. Although such a magnetic field breaks the time-reversal symmetry, the energy spectrum is still doubly degenerate due to the C_{2x} symmetry of the system. Gapless edge modes arise inside the bulk band gap, which is independent of the width of the zero-field region. However, when the Fermi level is located outside the bulk gap, we find that a pair of spin-polarized edge modes are located at sample boundaries propagating with the same direction. Based on the spin-polarized edge mode, a stable spin bias and spin current can be produced. In addition, a pair of spin-resolved snake states are induced to be localized near the zero-field region. We numerically show that these spin-polarized edge states and snake states are robust against the short-range Anderson disorder.

We gratefully acknowledge the financial support from NSF-China under Grants No. 11004046, No. 10974236, and No. 11174252, and the Natural Science Foundation of Hebei Province of China under Grants No. A2010000339 and No. A2012205071. Y.T.Z. would also like to thank Kai Chang for helpful discussions.

[1] C. L. Kane and E. J. Mele, Phys. Rev. Lett. **95**, 226801 (2005).
[2] C. Wu, B. A. Bernevig, and S.-C. Zhang, Phys. Rev. Lett. **96**, 106401 (2006).
[3] C. Xu and J. E. Moore, Phys. Rev. B **73**, 045322 (2006).
[4] C. L. Kane and E. J. Mele, Phys. Rev. Lett. **95**, 146802 (2005).
[5] M. Z. Hasan and C. L. Kane, Rev. Mod. Phys. **82**, 3045 (2010).
[6] X.-L. Qi and S.-C. Zhang, Rev. Mod. Phys. **83**, 1057 (2011).
[7] W. X. Feng, D. Xiao, J. Ding, and Y. G. Yao, Phys. Rev. Lett. **106**, 016402 (2011).
[8] H. Min, J. E. Hill, N. A. Sinitsyn, B. R. Sahu, L. Kleinman, and A. H. MacDonald, Phys. Rev. B **74**, 165310 (2006); Y. Yao, F. Ye, X.-L. Qi, S.-C. Zhang, and Z. Fang, *ibid.* **75**, 041401(R) (2007); M. Gmitra, S. Konschuh, C. Ertler, C. Ambrosch-Draxl, and J. Fabian, *ibid.* **80**, 235431 (2009).
[9] B. A. Bernevig, T. L. Hughes, and S. C. Zhang, Science **314**, 1757 (2006).
[10] M. König, S. Wiedmann, C. Brüe, A. Roth, H. Buhmann, L. W. Molenkamp, X. L. Qi, and S. C. Zhang, Science **318**, 766 (2007).
[11] Z. H. Qiao, W.-K. Tse, H. Jiang, Y. G. Yao, and Q. Niu, Phys. Rev. Lett. **107**, 256801 (2011); X. Li, Z. H. Qiao, J. Jung, and Q. Niu, Phys. Rev. B **85**, 201404(R) (2012).
[12] C.-C. Liu, W. X. Feng, and Y. G. Yao, Phys. Rev. Lett. **107**, 076802 (2011).
[13] Q.-F. Sun and X. C. Xie, Phys. Rev. Lett. **104**, 066805 (2010).
[14] I. Knez, R.-R. Du, and G. Sullivan, Phys. Rev. Lett. **107**, 136603 (2011).
[15] T. Yokoyama, Y. Tanaka, and N. Nagaosa, Phys. Rev. Lett. **102**, 166801 (2009).
[16] A. R. Akhmerov, C. W. Groth, J. Tworzydło, and C. W. J. Beenakker, Phys. Rev. B **80**, 195320 (2009).
[17] V. Krueckl and K. Richter, Phys. Rev. Lett. **107**, 086803 (2011).
[18] J. Li, R.-L. Chu, J. K. Jain, and S.-Q. Shen, Phys. Rev. Lett. **102**, 136806 (2009).
[19] H. Jiang, L. Wang, Q.-F. Sun, and X. C. Xie, Phys. Rev. B **80**, 165316 (2009).
[20] W. Li, J. Zang, and Y. Jiang, Phys. Rev. B **84**, 033409 (2011).
[21] C. W. Groth, M. Wimmer, A. R. Akhmerov, J. Tworzydło, and C. W. J. Beenakker, Phys. Rev. Lett. **103**, 196805 (2009).
[22] Y. X. Xing, L. Zhang, and J. Wang, Phys. Rev. B **84**, 035110 (2011).
[23] K. Chang and W.-K. Lou, Phys. Rev. Lett. **106**, 206802 (2011).
[24] Q.-F. Sun, Y.-X. Li, W. Long, and J. Wang, Phys. Rev. B **83**, 115315 (2011).
[25] J. Maciejko, X.-L. Qi, and S.-C. Zhang, Phys. Rev. B **82**, 155310 (2010).
[26] G. Tkachov and E. M. Hankiewicz, Phys. Rev. Lett. **104**, 166803 (2010).
[27] J.-C. Chen, J. Wang, and Q.-F. Sun, Phys. Rev. B **85**, 125401 (2012).
[28] M. König, H. Buhmann, L. W. Molenkamp, T. L. Hughes, C.-X. Liu, X.-L. Qi, and S.-C. Zhang, J. Phys. Soc. Jpn. **77**, 031007 (2008).
[29] C.-X. Liu, X.-L. Qi, X. Dai, Z. Fang, and S.-C. Zhang, Phys. Rev. Lett. **101**, 146802 (2008).
[30] C. Brüne, A. Roth, H. Buhmann, E. M. Hankiewicz, L. W. Molenkamp, J. Maciejko, X.-L. Qi, and S.-C. Zhang, Nat. Phys. **8**, 486 (2012).
[31] J. E. Müller, Phys. Rev. Lett. **68**, 385 (1992).
[32] N. Nemec and G. Cuniberti, Phys. Rev. B **74**, 165411 (2006).
[33] H. W. Lee and D. S. Novikov, Phys. Rev. B **68**, 155402 (2003).
[34] L. Oroszlany, P. Rakyta, A. Kormanyos, C. J. Lambert, and J. Cserti, Phys. Rev. B **77**, 081403(R) (2008).
[35] T. K. Ghosh, A. De Martino, W. Häusler, L. Dell'Anna, and R. Egger, Phys. Rev. B **77**, 081404(R) (2008).
[36] J. R. Williams and C. M. Marcus, Phys. Rev. Lett. **107**, 046602 (2011).
[37] *Electronic Transport in Mesoscopic Systems*, edited by S. Datta (Cambridge University Press, Cambridge, UK, 1995).
[38] D. H. Lee and J. D. Joannopoulos, Phys. Rev. B **23**, 4997 (1981).
[39] X. C. Zhang, A. Pfeuffer-Jeschke, K. Ortner, V. Hock, H. Buhmann, C. R. Becker, and G. Landwehr, Phys. Rev. B **63**, 245305 (2001).